Analysis of the Electron Paramagnetic Resonance Properties of the [2Fe-2S]$^{1+}$ Centers in Molybdenum Enzymes of the Xanthine Oxidase Family: Assignment of Signals I and II

Jorge Caldeira,[‡,§] Valérie Belle,[||] Marcel Asso,[||] Bruno Guigliarelli,[||] Isabel Moura,[§] José J. G. Moura,[§] and Patrick Bertrand*[,||]

Instituto Superior de Ciências da Saùde-Sul and Departamento de Quimica, Centro de Quimica Fina e Biotecnologia, Faculdade de Ciências e Tecnologia, Universidade Nova de Lisboa, 2825-114 Caparica, Portugal, Laboratoire de Bioénergétique et Ingénierie des Protéines, Institut de Biologie Structurale et Microbiologie, Centre National de la Recherche Scientifique, 31 Chemin Joseph Aiguier, 13402 Marseille Cedex 20, France, and Université de Provence, 13331 Marseille Cedex 3, France

Received September 15, 1999; Revised Manuscript Received December 9, 1999

ABSTRACT: Molybdoenzymes of the xanthine oxidase family contain two [2Fe-2S]$^{1+,2+}$ clusters that are bound to the protein by very different cysteine motifs. In the X-ray crystal structure of *Desulfovibrio gigas* aldehyde oxidoreductase, the cluster ligated by a ferredoxin-type motif is close to the protein surface, whereas that ligated by an unusual cysteine motif is in contact with the molybdopterin [Romao, M. J., Archer, M., Moura, I., Moura, J. J. G., LeGall, J., Engh, R., Schneider, M., Hof, P., and Huber, R. (1995) *Science 270*, 1170−1176]. These two clusters display distinct electron paramagnetic resonance (EPR) signals: the less anisotropic one, called signal I, is generally similar to the $g_{av} \approx 1.96$-type signals given by ferredoxins, whereas signal II often exhibits anomalous properties such as very large *g* values, broad lines, and very fast relaxation properties. A detailed comparison of the temperature dependence of the spin−lattice relaxation time and of the intensity of these signals in *D. gigas* aldehyde oxidoreductase and in milk xanthine oxidase strongly suggests that the peculiar EPR properties of signal II arise from the presence of low-lying excited levels reflecting significant double exchange interactions. The issue raised by the assignment of signals I and II to the two [2Fe-2S]$^{1+}$ clusters was solved by using the EPR signal of the Mo(V) center as a probe. The temperature dependence of this signal could be quantitatively reproduced by assuming that the Mo(V) center is coupled to the cluster giving signal I in xanthine oxidase as well as in *D. gigas* aldehyde oxidoreductase. This demonstrates unambiguously that, in both enzymes, signal I arises from the center which is closest to the molybdenum cofactor.

Some molybdenum-containing enzymes catalyze the oxidative hydroxylation of aldehydes and aromatic heterocycles. Spectroscopic studies have shown that, besides the molybdenum cofactor which constitutes their active site, these proteins contain two [2Fe-2S]$^{1+,2+}$ clusters and often a FAD[1] group (*1*). A well-known member of this family is the eukaryotic protein xanthine oxidase, but related enzymes such as aldehyde oxidoreductases (AOR) and CO dehydrogenases have been found in a variety of bacteria. The highly homologous amino acid sequences of these proteins suggest similar arrangements of the prosthetic groups. In particular, all these sequences contain two conserved groups of cysteines liable to coordinate the Fe−S clusters: a C-X_4-C-X_2-C-X_n-C motif identical to that found in plant-type ferredoxins and a C-X_2-C-X_n-C-X-C motif, which is currently unique among iron−sulfur proteins (*1*). The involvement of these cysteines in the ligation of the Fe−S clusters has been confirmed by the resolution of the X-ray crystal structure of *Desulfovibrio gigas* AOR. In this protein, the cluster ligated by the "regular" cysteine motif is close to the protein surface and is located in a domain displaying a chain fold very similar to that found in plant-type ferredoxins. In contrast, the cluster ligated by the unusual cysteine motif lies in a domain with a very different structure, is deeply buried, and is in contact with the molybdopterin (*2*). In the following, the two [2Fe-2S] clusters will be called distal and proximal according to their location with respect to the active site (Figure 1).

In their reduced form, the two [2Fe-2S]$^{1+}$ clusters of molybdenum hydroxylases exhibit distinct EPR signatures: the less anisotropic signal called signal I is characterized by *g* values, line widths and relaxation behavior that are similar to those of the $g_{av} \approx 1.96$-type signals displayed by [2Fe-2S]$^{1+}$ clusters in ferredoxins, whereas signal II often exhibits unusual properties such as very anisotropic *g* values, broad lines, and very fast relaxation properties *(3−11)*. Assuming a direct link between the spectral characteristics and the arrangement of the coordinating cysteines in the sequence led some authors to conclude that signal I arises from the

[†] This work was supported in part by the ICCTI/CNRS exchange program.

* Corresponding author: Fax (33) 4 91 16 45 78; E-mail bertrand@ibsm.cnrs-mrs.fr.

[‡] Instituto Superior de Ciências da Saùde-Sul.

[§] Universidade Nova de Lisboa.

[||] Institut de Biologie Structurale et Microbiologie, CNRS, and Université de Provence.

[1] Abbreviations: EPR, electron paramagnetic resonance; ENDOR, electron nuclear double resonance; AOR, aldehyde oxidoreductase; FAD, flavin adenin dinucleotide.

10.1021/bi9921485 CCC: $19.00
Published on Web 02/15/2000

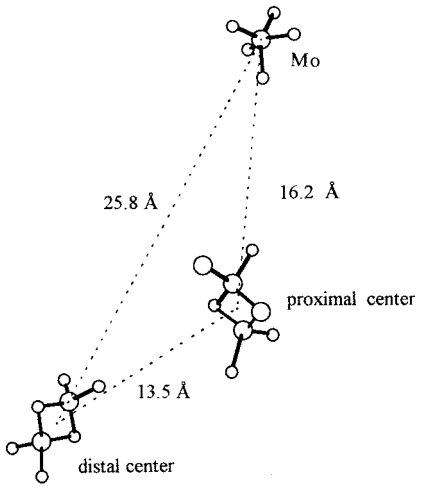

FIGURE 1: Relative arrangement of the metal centers given by the X-ray crystal structure of *D. gigas* AOR.

distal cluster and that the anomalous EPR properties of signal II reflect the peculiar arrangement of the cysteines coordinating the proximal cluster (*12*). This assignment was supported by a preliminary report on ENDOR experiments carried out on milk xanthine oxidase, which suggests that the cluster responsible for signal I is more solvent-exposed than that giving signal II (*13*). It is in conflict, however, with other experiments carried out on the same enzyme, which have shown that when the molybdenum center is in the paramagnetic Mo(V) form, it interacts magnetically only with the [2Fe-2S]$^{1+}$ cluster giving signal I (*14*−*16*).

This confused situation urged us to examine more thoroughly the EPR properties of the [2Fe-2S] clusters of molybdenum hydroxylases. When these properties are compared to those observed in other [2Fe-2S]-containing proteins, it appears that the characteristics of signal II are anomalous only in certain of these enzymes. Besides, a detailed analysis shows that the EPR characteristics of [2Fe-2S]$^{1+}$ clusters are not necessarily related to the sequence of their coordinating cysteines. Therefore, it is not possible to assign reliably signals I and II to the two cysteine motifs present in the enzymes of the xanthine oxidase family. However, by using the EPR signal displayed by the Mo(V) center as a probe, it is possible to take advantage of the different relaxation properties of signals I and II to decide unambiguously which signal arises from the proximal cluster.

MATERIALS AND METHODS

In the sample of milk xanthine oxidase used in this work, the Mo(V) species was in the desulfo-inhibited form. Its preparation has been described previously (*16*). *D. gigas* AOR was isolated and purified as described (*17*). The sample concentration was 0.21 mM in 10 mM deuterated phosphate buffer (pH 7.5). It was reduced anaerobically by sodium dithionite. X-band EPR spectra were recorded on a Bruker ESP 300E spectrometer. The samples were cooled with an Oxford Instrument ESR 900 cryostat fitted with an ITC 503 temperature controller. Q-band spectra were recorded by using a ER051QG microwave bridge and a CF935 cryostat.

Spin−*Lattice Relaxation and Intensity Measurements.* The spin−lattice relaxation times T_1 characterizing signals I and II in *D. gigas* AOR and xanthine oxidase were deduced from the relaxation broadening of their low-field (g_z) peaks. The half-width $\delta_L(T) = \hbar/(g\beta T_1)$ of the Lorentzian relaxation component was determined by using the method presented in ref *18*, which enables the deconvolution of the relaxation component of an EPR line inhomogeneously broadened by unresolved hyperfine or spin−spin interactions.

In both enzymes, the temperature dependence of the intensity of signals I and II was studied by monitoring the amplitude of their g_z peaks. When necessary, this amplitude was corrected to account for relaxation broadening. The relaxation and intensity measurements were carried out at Q-band for signals I and II in *D. gigas* AOR and for signal I in xanthine oxidase. In the case of the very broad signal II exhibited by xanthine oxidase, the line width measurements proved to be very sensitive even to weak baseline distortions, and more accurate results were obtained by recording the spectrum at X-band. Multifrequency experiments carried out on signals I and II in *D. gigas* AOR and signal I in xanthine oxidase have shown that the temperature dependence of δ_L and of the intensity are identical at X-band and at Q-band.

Analysis of the Temperature Dependence of the Spectrum Given by the Spin-Coupled Mo(V) Center. The variation in the shape of the Mo(V) interaction spectrum as a function of temperature is governed by the temperature dependence of the T_1 of the interacting [2Fe-2S]$^{1+}$cluster. This phenomenon can be quantitatively described by using the formalism developed in the analogous problem of chemical exchange in the context of NMR spectroscopy. When the standard expression giving the NMR line shape in the presence of chemical exchange (*19*) is adapted to describe the shape $s(B)$ of the split EPR line, one obtains:

$$s(B) = (1 + T_1/T_2)(P + QR)/(P^2 + R^2) \qquad (1)$$

with $P = T_1[(1/T_2)^2 + \gamma^2(\Delta B/2)^2 - \gamma^2(B - B_u)^2] + (1/T_2)$, $Q = \gamma T_1(B - B_u)$, $R = \gamma(1 + 2T_1/T_2)(B - B_u)$, and $\gamma = g\beta/\hbar$. In this expression, B_u indicates the position of the unsplit line of the Mo(V) center, T_2 its spin−spin relaxation time, ΔB the splitting due to the spin−spin interactions with the proximal [2Fe-2S]$^{1+}$ cluster and T_1 the spin−lattice relaxation time of this cluster. When T_1 is anisotropic, the value to be used in eq 1 is that corresponding to the orientation of the magnetic field which gives a Mo(V) resonance line at B_u. Careful examination of the shape of signals I and II in the temperature range where the broadening of the spectrum is due to the shortening of T_1 suggests that the anisotropy of T_1 is weak. This was confirmed by detailed measurements carried out at the turning points of signals I in *D. gigas* AOR and xanthine oxidase, which showed that this anisotropy does not exceed a factor of 2. We have therefore used in the calculation the T_1 values deduced from the low-field (g_z) peaks of both signals. Equation 1 is equivalent to the expression describing the shape of the Mössbauer spectrum in the presence of a fluctuating environment (*20*). The spin−spin relaxation time T_2 of the Mo(V) center was determined via continuous-wave power-saturation experiments carried out at 50 and 80 K. A set of theoretical saturation curves was first calculated by assuming that the saturated spectrum results from the convolution of the unsaturated spectrum, considered as the spectral envelope describing the inhomogeneous broadening, and a saturated Lorentzian spin-packet characterized by its half-width δB_p (*21*). The value of δB_p was then determined

Table 1: Spectral Characteristics of the EPR Spectra Displayed by [2Fe-2S]$^{1+}$ Centers in Enzymes of the Xanthine Oxidase Family[a]

enzyme	signal I	signal II
milk xanthine oxidase[b]	1.894, 1.932, 2.022 (90 K)[c]	1.902, 1.991, 2.11 (60 K)[c]
turkey liver xanthine dehydrogenase[d]	1.906, 1.932, 2.017 (nr)	1.92, 2.00, 2.08 (<50 K)
rabbit liver aldehyde oxidoreductase[e]	1.918, 1.930, 2.018 (>70 K)	1.915, 2.003, 2.106 (60 K)
D. melanogaster xanthine dehydrogenase[f]	1.902, 1.933, 2.022 (nr)	1.896, 2.005, 2.118 (nr)
H. pseudoflava CO dehydrogenase[g]	1.905, 1.947, 2.023 (>80 K)[h]	1.873, 1.974, 2.160 (<50 K)
C. testosteroni aldehyde dehydrogenase[i]	1.904, 1.941, 2.023 (nr)	1.895, 1.980, 2.092 (<50 K)
P. putida quinoline 2-oxidoreductase[j]	1.898, 1.950, 2.035 (nr)	1.866, 1.970, 2.072 (nr)
P. diminuta isoquinoline 1-oxidoreductase[j]	1.919, 1.945, 2.010 (>77 K)	1.90, 1.974, 2.084 (<40 K)
Arthrobacter quinaldine 4-oxidoreductase[j]	1.937, 1.937, 2.02 (>77 K)	1.874, 1.983, 2.075 (<60 K)
D. gigas aldehyde oxidoreductase[c]	1.919, 1.938, 2.020 (100 K)	1.900, 1.97, 2.057 (90 K)

[a] The g values of signals I and II are given for each protein. In the text, these values are labeled according to $g_x < g_y < g_z$. The temperature at which the spectrum disappears at X-band is given in parentheses. [b] Reference *3*. [c] This work. [d] Reference *4*. [e] Reference *5*. [f] Reference *6*. [g] Reference *7*. [h] Reference *10*. [i] Reference *8*. [j] Reference *9*.

by fitting the set of calculated curves to the experimental saturation curve, and T_2 was deduced from the relation $1/T_2 = g\beta\delta B_p/\hbar$. Finally, the Mo(V) interaction spectrum was calculated as the convolution of the function $s(B)$ given by eq 1 and a Gaussian envelope describing the inhomogeneous broadening.

RESULTS

Variation of Signals I and II among the Family of Molydenum Hydroxylases. For a given enzyme, signals I and II are defined only with respect to each other: the less anisotropic and the more anisotropic signals are labeled I and II, respectively. To appreciate whether this labeling reflects the existence of two distinct groups, it is necessary to examine how these signals vary among the family of molybdenum hydroxylases. The g values measured in signals I and II in enzymes of the xanthine oxidase family are reported in Table 1, and their variations as a function of the difference $g_y - g_x$ ($g_x < g_y < g_z$) are plotted in Figure 2. This representation shows that the sets of g values corresponding to signals I and II do not overlap, which confirms that they belong to two groups differing by the anisotropy of the **g** tensor. Large fluctuations are, however, observed within each group, and the gap between the two groups is not large: the g values of signal I in quinoline 2-oxidoreductase from *Pseudomonas putida* do not differ much from those of signal II in *D. gigas* AOR (Table 1). In general, the variations in the g values of signal I follow the trend observed in [2Fe-2S] proteins giving a $g_{av} \approx 1.96$-type EPR spectrum, although significant departures are observed in the case of xanthine oxidase and xanthine dehydrogenases from turkey liver and *Drosophila melanogaster* (Figure 2). The g values of signal II exhibit much more pronounced fluctuations: in some proteins such as *D. gigas* AOR, *P. putida* quinoline 2-oxireductase, and *Arthrobacter* quinaldine 4-oxidase, the g values are close to those expected in the $g_{av} \approx 1.96$ class, whereas unusually large values are observed in other enzymes such as xanthine oxidase, *Pseudomonas diminuta* isoquinoline 1-oxidoreductase, xanthine dehydrogenases from turkey liver and *D. melanogaster*, *Comamonas testosteroni* aldehyde dehydrogenase, rabbit liver aldehyde oxidoreductase, and *Hydrogenophaga pseudoflava* CO dehydrogenase (Figure 2). Remarkably, those signals that display unusual g values disappear above about 50 K (Table 1). To elucidate the cause of this disappearance, we have compared the temperature dependence of the spin−lattice relaxation time T_1 and of the intensity of signals I and II in xanthine oxidase and in *D. gigas* AOR.

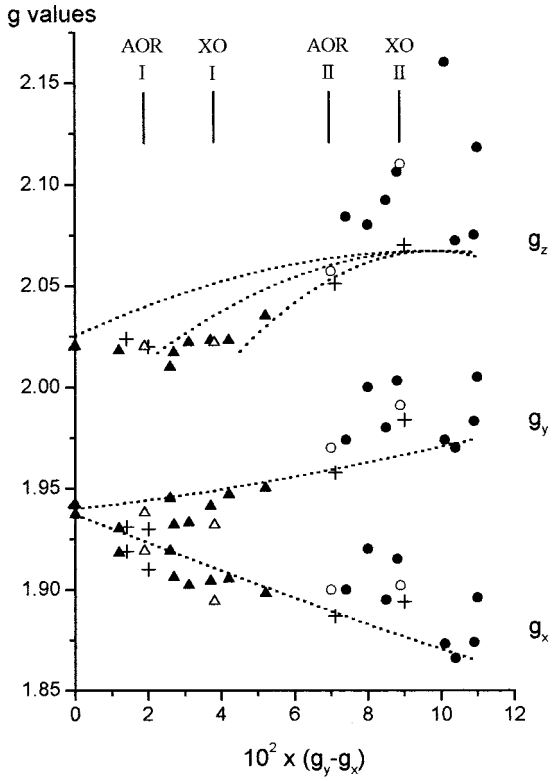

FIGURE 2: g values of [2Fe-2S]$^{1+}$ centers in proteins of the xanthine oxidase family, plotted as a function of the difference $g_y - g_x$ ($g_x < g_y < g_z$). The data given in Table 1 are shown as solid triangles and solid circles for signals I and II, respectively, except those concerning *D. gigas* AOR and xanthine oxidase, which are shown as open symbols. Plus signs correspond to the g values measured in other proteins, which are given for comparison: from left to right, *E. coli* fumarate reductase, NIFU protein from *A. vinelandii*, *Spirulina maxima* ferredoxin, and ferredoxin from *Halobacterium* of the Dead Sea. The calculated lines, which are the best fit to the data obtained in proteins giving an EPR spectrum of the $g_{av} \approx 1.96$ type, are identical to those given in Figure 1 in ref *22*.

Temperature Dependence of the Spin−Lattice Relaxation Time and of the Intensity. The spin−lattice relaxation times of the centers giving signals I and II in *D. gigas* AOR and xanthine oxidase were deduced from the relaxation broadening of their low-field g_z peaks (Figure 3). In *D. gigas* AOR, the spin−spin interactions between the two [2Fe-2S]$^{1+}$ clusters give rise to a splitting of the g_z peak of signal I, which is resolved at X-band (*11*) but not at Q-band (Figure 3). Therefore, the relaxation broadening experiments were preferentially conducted at Q-band, except in the case of signal II of xanthine oxidase, which was studied at X-band

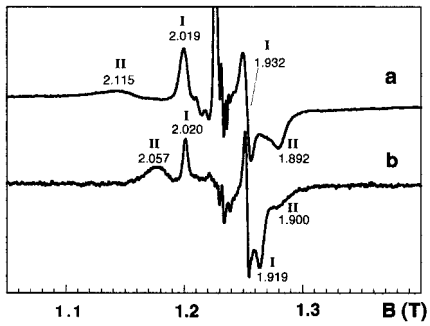

FIGURE 3: Q-band EPR spectra displayed by the fully reduced form of (a) milk xanthine oxidase and (b) *D. gigas* AOR. Experimental conditions: temperature, 20 K; microwave frequency, (a) 34.01 GHz or (b) 34.02 GHz; modulation amplitude, 1 mT; microwave power, (a) 0.4 mW or (b) 0.04 mW. Spectral features connected with signals I and II are indicated.

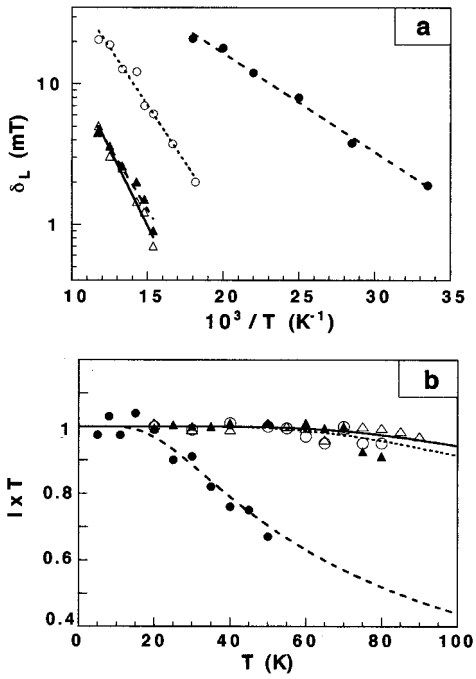

FIGURE 4: (a) Temperature dependence of the half-width δ_L of the Lorentzian relaxation component of signals I and II in *D. gigas* AOR and xanthine oxidase. The calculated lines are the best fits obtained with the relation $\delta_L \propto \exp(-\Delta/k_BT)$, with $\Delta = 330$ cm^{-1} (—), 240 cm^{-1} (•••), or 90 cm^{-1} (- - -). (b) Temperature dependence of the intensity of signals I and II in *D. gigas* AOR and xanthine oxidase. The normalized value of the product IT was obtained by measuring the area of the g_z peak. The calculated lines are the best fits obtained with eq 2, giving the temperature dependence of the intensity of the EPR signal displayed by the $S = {}^1/_2$ ground state of a [Fe(III), Fe(II)] system in which the exchange interactions are described by $-2JS_1S_2$, with $-J = 85$ cm^{-1} (—), 65 cm^{-1} (•••), or 20 cm^{-1} (- - -). In both figures, the following symbols have been used: (△) signal I in *D. gigas* AOR; (▲) signal I in xanthine oxidase; (○) signal II in *D. gigas* AOR; (●) signal II in xanthine oxidase.

(see Materials and Methods). The temperature dependence of the half-width δ_L of the Lorentzian relaxation component of signal I and signal II in xanthine oxidase and *D. gigas* AOR are shown in Figure 4a. These variations are well fitted by the equation $\delta_L \propto \exp(-\Delta/k_BT)$, corresponding to an Orbach process involving an excited state of energy Δ (*22*), with $\Delta = 330 \pm 30$ cm^{-1} in the case of signal I in *D. gigas* AOR (Figure 4a, △), $\Delta = 240 \pm 30$ cm^{-1} in the case of signal II in *D. gigas* AOR and signal I in xanthine oxidase

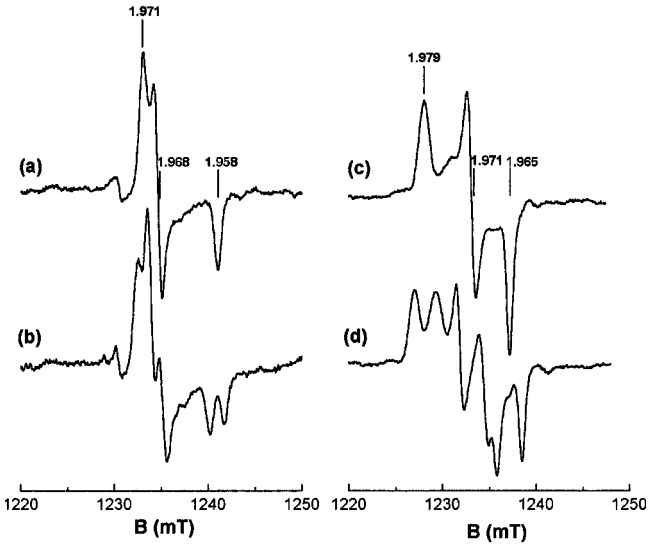

FIGURE 5: Low-temperature and high-temperature forms of the Q-band EPR spectrum (slow signal) displayed by the Mo(V) center in D_2O in (a, b) *D. gigas* AOR and (c, d) milk xanthine oxidase. Experimental conditions: temperature, (a, c) 100 K or (b, d) 30 K; microwave frequency, (a, b) 33.98 GHz or (c, d) 33.94 GHz; microwave power, (a) 100 μW, (b) 0.88 μW, (c) 43 μW, or (d) 4.3 μW; modulation frequency, (a) 100 kHz or (b−d) 1.56 kHz; modulation amplitude, (a, c, d) 0.21 mT or (b) 0.45 mT.

(Figure 4a, ○ and ▲), and $\Delta = 90 \pm 20$ cm^{-1} in the case of signal II in xanthine oxidase (Figure 4a, ●). The intensity of the g_z peaks of signals I and II in *D. gigas* AOR and xanthine oxidase is plotted as a function of temperature in Figure 4b. The data were fitted by

$$IT/I_0T_0 = 1/(1 + 2x^3 + 3x^8 + 4x^{15} + 5x^{24}) \qquad (2)$$

where $x = \exp(J/kT)$, which gives the temperature dependence of the intensity of the EPR signal displayed by the $S = {}^1/_2$ ground state of a system where a ferric ($S_1 = {}^5/_2$) and a ferrous ($S_2 = 2$) ions are coupled by exchange interactions described by $-2J\vec{S}_1\vec{S}_2$. $|J| = 85 \pm 10$ cm^{-1} was obtained in the case of signal I in *D. gigas* AOR (Figure 4b, △), while $|J| = 65 \pm 10$ cm^{-1} was obtained in the case of signal I in xanthine oxidase and signal II in *D. gigas* AOR (Figure 4b, ▲ and ○). In contrast, the temperature dependence displayed by signal II in xanthine oxidase could be reproduced only by using a very small $|J|$ value of about 20 cm^{-1} (Figure 4b, ●).

Temperature Dependence of the Split Mo(V) Spectrum. The enzymes of the xanthine oxidase family can be prepared in a redox state in which a significant fraction of the molybdenum atoms are present in the paramagnetic Mo(V) form. When the redox state of the enzyme is such that the Mo(V) center is in the presence of paramagnetic [2Fe-2S]$^{1+}$ centers, a split Mo(V) EPR signal is observed at low temperatures (Figure 5b,d). Upon raising the temperature, the splitting progressively disappears until an unsplit signal is finally observed above about 100 K (Figure 5a,c). This temperature behavior indicates that the Mo(V) center is coupled by spin−spin interactions to one or both Fe−S clusters: at low temperatures, the spin−lattice relaxation rate $1/T_1$ of these clusters is small compared to the splitting expressed in frequency units, and the split spectrum is observed, whereas the shortening of T_1 causes the spin−

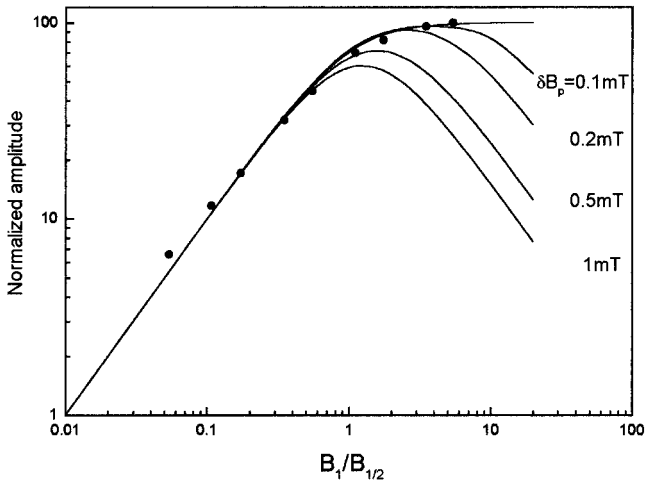

FIGURE 6: Determination of the spin−spin relaxation time T_2 of the Mo(V) center in *D. gigas* AOR from the shape of the saturation curve at 50 K. (●) Amplitude measured at the center of the split g_x line plotted as a fonction of the squared root of the microwave power. Theoretical curves giving the normalized amplitude as a function of the $B_1/B_{1/2}$ ratio, where B_1 is the microwave field amplitude and $B_{1/2} = (\hbar\delta B_p/g\beta T_1)^{1/2}$, were calculated for various values of the spin−packet line width δB_p as explained under Materials and Methods.

spin interactions to be averaged out at high temperatures. Since the shape of the split Mo(V) spectrum is typical of a coupling with a single paramagnetic center, its temperature dependence is governed by that of the T_1 of this center. To identify which Fe−S center is coupled to the Mo(V) center, we have used the model presented in the Materials and Methods section to simulate the shape of the Mo(V) spectrum of xanthine oxidase and *D. gigas* AOR in the 30−80 K range, by successively using the T_1 values measured for signals I and II (Figure 4a). In the case of *D. gigas* AOR, the study was carried out in the high-field part of the Q-band spectrum where the resolution is the highest and the splitting ΔB is equal to 1.5 mT (Figure 5b). In the case of xanthine oxidase, the highest resolution was obtained in the low-field part of the Q-band spectrum, where a ΔB value equal to 2.3 mT was measured (Figure 5d). Saturation experiments carried out in the high-field part of the Mo(V) spectrum of *D. gigas* AOR have shown that T_2 is sufficiently long that the spin-packet halfwidth δB_p is smaller than 0.1 mT at 50 K (Figure 6) and 80 K (data not shown). In these circumstances, it can be shown that $1/T_2$ can be neglected in eq 1. To account for the inhomogeneous broadening of the Mo(V) line, the spectrum was calculated as the convolution of the function s(B) given by eq1 and a Gaussian envelope. The line width of this envelope was chosen so as to reproduce the shape of the unsplit peak visible in the high-temperature Mo(V) spectrum (Figure 5a,c). At 100 K, the line widths of the high-field peak of the spectrum given by *D. gigas* AOR (Figure 5a) and of the low-field peak of the spectrum given by xanthine oxidase (Figure 5c) were found to be equal to 0.8 and 1.4 mT, respectively.

The temperature dependence of the split Mo(V) signal calculated by using the T_1 values corresponding to signals I and II is compared to that observed experimentally in *D. gigas* AOR and xanthine oxidase in Figures 7 and 8, respectively. It turns out that the temperature dependence of the split Mo(V) center is perfectly reproduced in both enzymes by assuming that the interacting $[2Fe\text{-}2S]^{1+}$ cluster is that giving signal I. If one considers the great sensitivity of the calculated shape with respect to the T_1 value, the agreement is indeed remarkable. In particular, the fact that the collapse of the split line occurs at 65 K in both enzymes is nicely reproduced by the model. This result could not be anticipated, since several parameters involved in the calculation differ in *D. gigas* AOR and xanthine oxidase, like the splitting and the inhomogeneous broadening of the Mo(V) signal and the relaxation time of signal I (Figures 4a and 5). When the Mo(V) center of *D. gigas* AOR was assumed to be coupled to the cluster giving signal II, the collapse took place at 40 K, in clear contradiction with experiment (Figure 7). In the case of xanthine oxidase, the T_1 value corresponding to signal II could not be measured at Q-band. However, when the T_1 values measured at X-band were used in eq 1, the collapse was predicted to occur at 25 K (data not shown). Since T_1 is shorter at Q-band than at X-band (*23*), the temperature at which the collapse takes place would be still lower if T_1 values measured at Q-band were used in the calculation. Another argument against the Mo(V) center being coupled to the Fe−S cluster giving signal II in xanthine oxidase is that the shape of the split Mo(V) spectrum does not change between 20 and 50 K even though excited spin states of this cluster become populated in this temperature range, as shown by the intensity measurements (Figure 4b).

DISCUSSION

To analyze the data shown in Figures 2−4, it is helpful to briefly recall the main features of the electronic structure of $[2Fe\text{-}2S]^{1+}$ clusters in proteins. In these clusters, the energies of the various spin states are determined by the interplay of several contributions: the strong antiferromagnetic coupling between the ferric ($S_1 = {}^5/_2$) and ferrous ($S_2 = 2$) iron ions mediated by the two bridging sulfurs, which can be described by the Heisenberg Hamiltonian $-2J\vec{S}_1\vec{S}_2$, the double exchange interaction arising from the valence delocalization phenomenon, which gives a $B(S + {}^1/_2)$ term, and the vibronic coupling energy U (*22*, *24*). In general, the ground state of $[2Fe\text{-}2S]^{1+}$ clusters is a spin doublet that gives an EPR spectrum characterized by $g_{av} \approx 1.96$ or $g_{av} \approx 1.91$. The first value is observed when the cluster is ligated only by cysteine residues, while the second is observed in Rieske-type centers in which the Fe(II) ion is ligated by two histidines (*22*). These g values are easily accounted for by use of

$$g = {}^7/_3\mathbf{g}_1 - {}^4/_3\mathbf{g}_2 \qquad (3)$$

where $\mathbf{g}_1$ and $\mathbf{g}_2$ are the $\mathbf{g}$ tensors of the ferric and ferrous sites, respectively. On the basis of eq 3, the variations in the g values observed within both classes can be rationalized by assuming that they arise mainly from a peculiar distortion of the Fe(II) site whose magnitude varies from one protein to another. Actually, eq 3 is valid only when the ground doublet is well separated from excited states, which requires the B/J ratio to be moderate (*22*). This condition is apparently met in all $[2Fe\text{-}2S]^{1+}$ centers in which the temperature dependence of the EPR signal has been studied so far: no departures from Curie's law were detected at low temperatures, and the relaxation broadening due to an Orbach process involving the first excited level was observed above about 60 K (*22*). In these circumstances, the energy of the first excited level lies at $\Delta = 3J$, and the magnitude of J can be

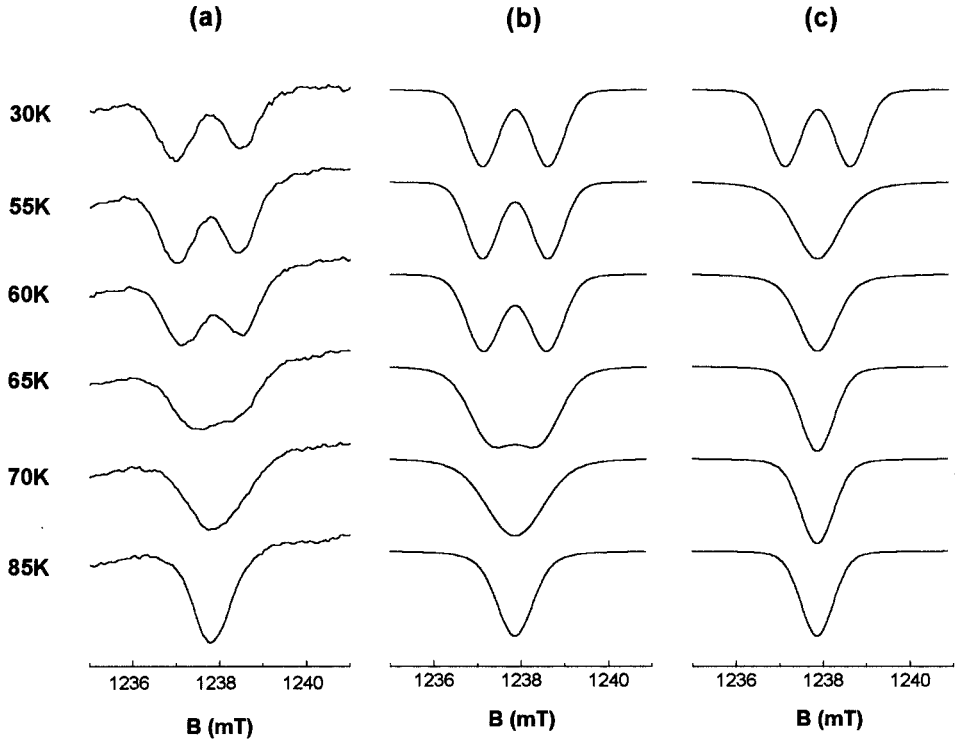

FIGURE 7: (a) Temperature dependence of the shape of the high-field peak ($g = 1.958$) in the EPR spectrum displayed by the Mo(V) center in *D. gigas* AOR; (b, c) Temperature dependence calculated with eq 1 by assuming that the splitting arises from the coupling with the $[2Fe\text{-}2S]^{1+}$ cluster giving signal I and II, respectively. The T_1 values used in the calculation were deduced from the line width δ_L of the relaxation component given in Figure 4a.

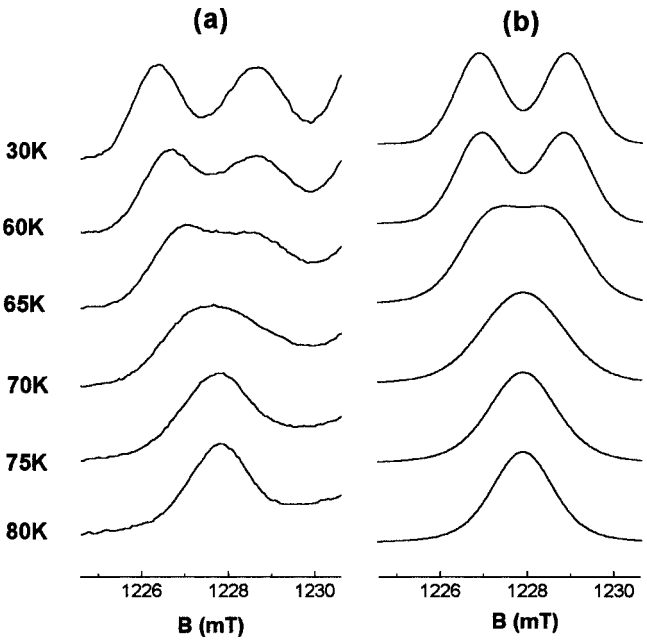

FIGURE 8: (a) Temperature dependence of the shape of the low-field peak ($g = 1.979$) in the EPR spectrum displayed by the Mo(V) center in xanthine oxidase. (b) Temperature dependence calculated with eq 1 by assuming that the splitting arises from the coupling with the $[2Fe\text{-}2S]^{1+}$ cluster giving signal I.

deduced from the temperature dependence of the magnetic susceptibility, of the EPR signal intensity, or of T_1. These methods yield $|J|$ values ranging from 70 to 170 cm^{-1} in various proteins (*22*). In other types of dinuclear clusters in which a ferric and a ferrous sites are linked by a μ-hydroxo bridge, the antiferromagnetic coupling is much weaker. As a consequence, the intensity of the signal arising from the $S = {}^1/_2$ ground state exhibits a strong departure from Curie's law (*25*) and eq 3 must be modified to include contributions due to mixing of low-lying excited states (*26*).

The EPR spectra given by $[2Fe\text{-}2S]^{1+}$ centers in molybdenum hydroxylases can be classified into two groups according to their anisotropy (Figure 2). In both groups, some proteins yield very similar g values to those found in the $g_{av} \approx 1.96$ class. This is observed in particular in the case of signals I and II in *D. gigas* AOR. The $|J|$ values equal to 85 ± 10 and 65 ± 10 cm^{-1} deduced from the temperature dependence of the intensity of signal I and II, respectively (Figure 4b), agree reasonably with the values $\Delta/3 = 110 \pm 10$ and 80 ± 10 cm^{-1} deduced from the relaxation experiments (Figure 4a) and are similar to those measured in other $[2Fe\text{-}2S]^{1+}$ clusters (*22*). Some proteins of the xanthine oxidase family give g values that depart moderately from those found in the $g_{av} = 1.96$ class (Figure 2). A moderate departure of this kind was already observed in proteins that do not belong to this family, such as *Escherichia coli* fumarate reductase, the NIFU protein from *Azotobacter vinelandii*, and the ferredoxin from *Halobacterium* of the Dead Sea (Figure 2). In these proteins, the temperature dependence of the EPR signal was found to be usual (*27*−*30*), suggesting that eq 3 is valid. Therefore, these peculiar g values most likely arise from a different distortion of the ferrous site. Since a large J value was deduced from the temperature dependence of the spin−lattice relaxation rate and of the intensity of signal I in xanthine oxidase (Figure 4), the same explanation probably applies in the case of those $[2Fe\text{-}2S]^{1+}$ centers of molybdenum hydroxylases whose g values are close to those of the $g_{av} = 1.96$ class.

In some enzymes of the xanthine oxidase family, such as *P. diminuta* isoquinoline-1-oxidoreductase, turkey liver xan-

thine dehydrogenase, *C. testosteroni* aldehyde dehydrogenase, CO dehydrogenase, rabbit liver AOR, xanthine oxidase, *H. pseudoflava* CO dehydrogenase, and *D. melanogaster* xanthine dehydrogenase, the electronic structure of the [2Fe-2S]$^{1+}$ center giving signal II seems to be markedly different: this signal is highly anisotropic and disappears above 50 K (Table 1). This anisotropy can hardly be explained on the basis of eq 3: taking ferrous **g** tensor components greater than 2.00 and ferric **g** tensor components in the 2.01−2.04 range expected for an Fe(III) ion with tetrahedral sulfur coordination (*22*) yields a maximum *g* value of 2.09, which is smaller than some *g* values reported in Table 1. The anomalous temperature dependence displayed by these signals, which results in their disappearance at very low temperatures, suggests that the failure of eq 3 is due to the presence of low-lying excited levels. This view is confirmed by the dramatic decrease in the intensity of signal II that is observed above 20 K in xanthine oxidase (Figure 4b). This decrease can be reproduced by using a Heisenberg Hamiltonian with $|J| = 20$ cm^{-1} (Figure 4b), a value that is roughly consistent with $\Delta/3 = 30$ cm^{-1} deduced from the relaxation experiments (Figure 4a). Such values seem, however, to be too small to account for the strong antiferromagnetic interactions mediated by the bridging sulfides of [2Fe-2S]$^{1+}$ clusters. A likely explanation is that the *B*/*J* ratio is larger in these clusters than in conventional [2Fe-2S]$^{1+}$ centers. In these circumstances, the spacing of the energy levels of the various spin states depends on *J*, *B*, and *U* (*22*). It should be noted that a sizable *B*/*J* ratio does not necessarily mean that the valences of the iron sites are delocalized in these clusters, since the degree of valence delocalization is governed by the magnitude of the *B*/*U* ratio (*22*). Mössbauer experiments have shown that the valences of the iron ions are trapped in the [2Fe-2S]$^{1+}$clusters of *D. gigas* AOR and xanthine oxidase (*3*, *31*). Large *B* values have been already invoked to explain the peculiar EPR and Mössbauer characteristics of the [2Fe-2S]$^{1+}$ clusters present in the C56S and C60S mutants of *Clostridium pasteurianum* ferredoxin (*32*, *33*) and in the [Fe_2S_2(dimethylmethanebisbenzimidazolate)$_2$]$^{3-}$ complex (*34*). In the former case, a large *B* value was needed to account for the $S = {}^9/_2$ ground state and the fully delocalized valences (*33*), whereas in the latter case a smaller value was shown to account for the relaxation properties and the partially delocalized valences (*34*). Further studies are in progress in our laboratories to determine the magnitude of the parameters *B*, *J*, and *U* in the [2Fe-2S]$^{1+}$ cluster giving signal II in xanthine oxidase.

Let us consider now the issue raised by the assignment of signals I and II in enzymes of the xanthine oxidase family. We have shown that these signals belong actually to two distinct groups (Figure 2). The fact that the cysteine motifs which bind the two clusters in *D. gigas* AOR are conserved in this family suggests that each motif corresponds to one group of signals. The nature of this correspondence is, however, unclear. As shown above, similar EPR signals to those observed in the $g_{av} = 1.96$ class are found in the group of signals I as well as in that of signals II (Figure 2). Indeed, the *g* values measured in signal II of *D. gigas* AOR are close to those of the [2Fe-2S]$^{1+}$cluster of *Spirulina maxima* ferredoxin (Figure 2). Anomalous EPR properties are, however, observed only in the case of the group of signals II. Concerning the relation between the EPR properties and the sequence of the cysteines in the binding motif, we first note that [2Fe-2S] centers coordinated by the same arrangement of cysteines can yield very different EPR signals: the binding motif C-X_4-C-X_2-C-X_n-C gives a rhombic spectrum in plant-type ferredoxins and an almost axial signal in the case of center 1 of *E. coli* fumarate reductase. These two signals are very similar to signals II and I of *D. gigas* AOR, respectively (Figure 2). Conversely, different binding motifs can give rise to similar EPR signals: the *g* values of center 1 in *E. coli* fumarate reductase are similar to those observed in the [2Fe-2S] ferredoxin from *C. pasteurianum* (*35*), in which the binding motif is C-X_n-C-X_m-C-X_3−C (*36*), and those given by the NIFU protein from *A. vinelandii*, in which the binding motif is C-X-C-X_n-C-X_2-C, symmetrical to the "unusual" binding motif of molybdenum hydroxylases (*28*). All these observations are easily understood in the framework of the above-mentioned ligand field model, in which the variation in the **g** tensor is mainly attributed to the variable distortion experienced by the Fe(II) site. This distortion depends on the geometry of the two cysteine residues ligating this site and is not expected to be uniquely determined by the sequence of the four coordinating cysteines.

From the preceding discussion, it can be concluded that signals I and II cannot be a priori assigned to the two binding motifs present in molybdenum hydroxylases. To assign these signals to the proximal and distal [2Fe-2S]$^{1+}$ clusters, we have therefore used a more direct method based on the different relaxation properties of the two signals and on the existence of spin−spin interactions between the Mo(V) center and one [2Fe-2S]$^{1+}$ cluster. This method shows unambiguously that the cluster interacting with the Mo(V) center is that giving signal I in *D. gigas* AOR as well as in xanthine oxidase (Figures 7 and 8). In the case of xanthine oxidase, the same assignment has been obtained by taking advantage of the large difference between the redox potentials of the two [2Fe-2S]$^{1+,2+}$ centers (*15*). These results, together with the relative arrangement of the metal centers displayed by the X-ray crystal structure of *D. gigas* AOR (Figure 1), lead to an assignment of signal I to the proximal center, which is bound by the unusual cysteine motif. If this assignment is extended to all the enzymes of the xanthine oxidase family, it is concluded that the cluster which exhibits anomalous EPR characteristics in certain of these enzymes (Table 1) is the distal one, which is bound by the plant-type cysteine motif. Since these properties are likely due to peculiar exchange interactions between the Fe(III) and Fe(II) sites of this cluster, their structural basis can be analyzed as soon as a high-resolution crystal structure of these proteins is available.

CONCLUSION

The results obtained in this study solve a long-standing issue with regard to the assignment of signals I and II in *D. gigas* AOR (*1*, *12*). More importantly, they open the way toward a detailed analysis of the intramolecular electron transfers in this protein. A straightforward application consists of assigning the redox potentials measured in potentiometric experiments monitored by EPR. In a previous study, signals I and II were reported to titrate at pH 7.6 with midpoint potentials equal to −280 and −285 mV, respectively (*37*). In a more recent study, more negative values equal to −365 mV for signal I and −330 mV for signal II were measured at pH 7.5, together with a moderate antico-

operative redox interaction of −20 mV (*38*). These data were found to be consistent with those obtained in spectrophotometric experiments carried out at room temperature (*38*). According to the assignment found in the present study, the $[2Fe\text{-}2S]^{2+,\ 1+}$ cluster characterized by the most negative potential is the proximal one in *D. gigas* AOR.

The assignment of the EPR signals to the two $[2Fe\text{-}2S]^{1+}$ clusters makes possible a detailed quantitative study of the intercenter spin−spin interactions. In *D. gigas* AOR, the spectrum displayed by the Mo(V) center is split by the spin−spin interactions with the proximal $[2Fe\text{-}2S]^{1+}$ center (Figure 5b), and the interactions between the two $[2Fe\text{-}2S]^{1+}$ clusters result in a splitting of the g_z peak of signal I, which is resolved at X-band (*11*). The numerical simulation of these interaction spectra based on the relative arrangement of the metal centers given by the X-ray crystal structure should provide useful information about the location of the reducible iron sites in both Fe−S clusters and the magnitude of the intercenter exchange interactions (*16*). Both points are important to elucidate the electron-transfer pathways in this protein.

ACKNOWLEDGMENT

We thank Professor Maria Joao Romao for providing the coordinates of the metal centers obtained in a recent high-resolution X-ray crystal study of *D. gigas* AOR.

REFERENCES

1. Hille, R. (1996) *Chem. Rev. 96*, 2757−2816.
2. Romao, M. J., Archer, M., Moura, I., Moura, J. J. G., Le Gall, J., Engh, R., Schneider, M., Hof, P., and Huber, R. (1995) *Science 270*, 1170−1176.
3. Hille, R., Hagen, W. R., and Dunham, W. R. (1985) *J. Biol. Chem. 260*, 10569−10575.
4. Barber, M. J., Bray, R. C., Lowe, D. J., and Coughlan, M. P. (1976) *Biochem. J. 153*, 297−307.
5. Barber, M., Coughlan, M. P., Rajagopalan, K. V., and Siegel, L. M. (1982) *Biochemistry 21*, 3561−3568.
6. Hughes, R. K., Bennett, B., and Bray, R. C. (1992) *Biochemistry 31*, 3073−3083.
7. Hänzelmann, P., and Meyer, O. (1998) *Eur. J. Biochem. 255*, 755−765.
8. Luykx, D. M., Duine, J. A., and de Vries, S. (1998) *Biochemistry 37*, 11366−11375.
9. Canne, C., Stephan, I., Finsterbusch, J., Lingens, F., Kappl, R., Fetzner, S., and Hüttermann, J. (1997) *Biochemistry 36*, 9780−9790.
10. Bray, R. C., George, N., Lange, R., and Meyer, O. (1983) *Biochem. J. 211*, 687−694.
11. Bray, R. C., Turner, N. A., Le Gall, J., Barata, B. A. S., and Moura, J. J. G. (1991) *Biochem. J. 280*, 817−820.
12. Romao, M. J., Knäblein, J., Huber, R., and Moura, J. J. G. (1997) *Prog. Biophys. Mol. Biol. 68*, 121−144.
13. Lowe, D. J., Mitchell, C. J., and Bray, R. C. (1997) *Biochem. Soc. Trans. 25*, 527S.
14. Lowe, D. J., and Bray, R. C. (1978) *Biochem. J. 169*, 471−479.
15. Barber, M. J., Salerno, J. C., and Siegel, L. M. (1982) *Biochemistry 21*, 1648−1656.
16. Bertrand, P., More, C., Guigliarelli, B., Fournel, A., Bennett, B., and Howes, B. (1994) *J. Am. Chem. Soc. 116*, 3078−3086.
17. Moura, J. J. G., Xavier, A. V., Bruschi, M., LeGall, J., Hall, D. O., and Cammack, R. (1976) *Biochem. Biophys. Res. Commun. 72*, 782−789.
18. Bertrand, P., Guigliarelli, B., Gayda, J.-P., Setif, P., and Mathis, P. (1988) *Biochim. Biophys. Acta 933*, 393−397.
19. Gutowsky, H. S., and Holm, C. H. (1956) *J. Chem. Phys. 25*, 1228−1234.
20. Leider, H. R., and Pipkorn, D. N. (1968) *Phys. Rev. 165*, 494−500.
21. Asso, M., Guigliarelli, B., Yagi, T., and Bertrand, P. (1992) *Biochim. Biophys. Acta 1122*, 50−56.
22. Guigliarelli, B., Bertrand, P. (1999) *Adv. Inorg. Chem. 47*, 53−129.
23. Orbach, R., and Stapleton, H. J. (1972) in *Electron Paramagnetic Resonance* (Geschwind, S., Ed.) pp 121−216, Plenum, New York.
24. Lamotte, B., and Mouesca, J.-M. (1997) *C. R. Acad. Sci. Paris 324*, 117−132.
25. Averill, B. A., Davis, J. C., Burman, S., Zirino, T., Sanders-Loehr, J., Loehr, T. M., Sage, J. T., and Debrunner, P. G. (1987) *J. Am. Chem. Soc. 109*, 3760−3767.
26. Guigliarelli, B., Bertrand, P., and Gayda, J.-P. (1986) *J. Chem. Phys. 85*, 1689−1692.
27. Werth, M. T., Cecchini, G., Manadori, A., Ackrell, B. A. C., Schröder, I., Gunsalus, R. P., and Johnson, M. K. (1990) *Proc. Natl. Acad. Sci. U.S.A. 87*, 8965−8969.
28. Fu, W., Jack, R. F., Morgan, T. V., Dean, D. R., and Johnson, M. K. (1994) *Biochemistry 33*, 13455−13463.
29. Werber, M. M., Bauminger, E. R., Cohen, S. G., and Ofer, S. (1978) *Biophys. Struct. Mech. 4*, 169−177.
30. Gayda, J.-P., Bertrand, P., More, C., and Cammack, R. C. (1981) *Biochimie 63*, 847−849.
31. Barata, B. A. S., Liang, J., Moura, I., Le Gall, J., Moura, J. J. G., and Huynh, B. H. (1992) *Eur. J. Biochem. 204*, 773−778.
32. Crouse, B. R., Meyer, J., and Johnson, M. K. (1995) *J. Am. Chem. Soc. 117*, 9612−9613.
33. Achim, C., Golinelli, M.-P., Bominaar, E. L., Meyer, J., and Münck, E. (1996) *J. Am. Chem. Soc. 118*, 8168−8169.
34. Ding, X.-Q., Bill, E., Trautwein, A. X., Winkler, H., Kostikas, A., Papaefthymiou, V., Simopoulos, A., Beardwood, P., and Gibson, J. F. (1993) *J. Chem. Phys. 99*, 6421−6428.
35. Fujinaga, J., and Meyer, J. (1993) *Biochem. Biophys. Res. Commun. 192*, 1115−1122.
36. Golinelli, M.-P., Akin, L. A., Crouse, B. R., Johnson, M. K., and Meyer, J. (1996) *Biochemistry 35*, 8995−9002.
37. Barata, B. A. S., Le Gall, J., and Moura, J. J. G. (1993) *Biochemistry 32*, 11559−11568.
38. More, C., Belle, V., Asso, M., Fournel, A., Roger, G., Guigliarelli, B., and Bertrand, P. (1999) *Biospectroscopy 5*, S3−S18.

BI9921485